Cell PRESS
Neuron
Article

Synaptic Ribbons Influence the Size and Frequency of Miniature-like Evoked Postsynaptic Currents

Bhupesh Mehta,[1,5] Josefin Snellman,[1,5] Shan Chen,[4] Wei Li,[4,*] and David Zenisek[1,2,3,*]
[1]Department of Cellular and Molecular Physiology
[2]Department of Ophthalmology and Visual Sciences
[3]Program in Cellular Neuroscience, Neurodegeneration and Repair
Yale University School of Medicine, Sterling Hall of Medicine, Room B147, New Haven, CT 06520, USA
[4]Unit on Retinal Neurophysiology, National Eye Institute Intramural Research Program, National Institute of Health, 35 Convent Drive, Room 2A-108, Bethesda, MD 20892, USA
[5]These authors contributed equally to this work
*Correspondence: liwei2@nei.nih.gov (W.L.), david.zenisek@yale.edu (D.Z.)
http://dx.doi.org/10.1016/j.neuron.2012.11.024

SUMMARY

Nonspiking cells of several sensory systems respond to stimuli with graded changes in neurotransmitter release and possess specialized synaptic ribbons. Here, we show that manipulations to synaptic ribbons caused dramatic effects on mEPSC-like (mIEPSC) amplitude and frequency. Damage to rod-bipolar cell ribbons using fluorophore-assisted light inactivation resulted in the immediate reduction of mIEPSC amplitude and frequency, whereas the first evoked response after damage remained largely intact. The reduction in amplitude could not be recovered by increasing release frequency after ribbon damage. In parallel experiments, we looked at mIEPSCs from cones of hibernating ground squirrels, which exhibit dramatically smaller ribbons than awake animals. Fewer and smaller mIEPSCs were observed postsynaptic to cones from hibernating animals, although depolarized cones were able to generate larger mIEPSCs. Our results indicate that ribbon size may influence mIEPSC frequency and support a role for ribbons in coordinating multivesicular release.

INTRODUCTION

In the visual, auditory, and vestibular systems, photoreceptors, bipolar cells, and hair cells have evolved to support tonic graded release of neurotransmitters in response to changes in sensory stimuli. These cells have specialized synaptic ribbons, proteinaceous structures to which dense arrays of vesicles are tethered (for review, see Matthews and Fuchs, 2010; Schmitz, 2009). In rod-bipolar cells (RBCs) of the retina, synaptic ribbons support both fast transient synaptic transmission, which signals temporal contrast, and tonic neurotransmitter release to signal luminance levels, which are detected as intermittent mEPSC-like events in postsynaptic Amacrine cells (Jarsky et al., 2011; Oesch and Diamond, 2011). Similarly, photoreceptors signal changes in light level as tonic changes in neurotransmitter release (Jackman et al., 2009).

Asynchronous mEPSC-like events emanating from several ribbon-type synapses have been shown to increase in size with depolarization (Li et al., 2009; Singer et al., 2004; however, see also Glowatzki and Fuchs, 2002). These large events are thought to arise from the near simultaneous release of the contents of multiple vesicles. To distinguish these from the mEPSCs that arise from the release of a single vesicle (Fatt and Katz, 1952), we refer to these here as miniature-like excitatory postsynaptic currents (mIEPSCs). The prevalence of multivesicular release from ribbon-type synapses suggests a possible role for the ribbon in facilitating these events.

Several studies have suggested a role for the ribbon in determining the size amount of neurotransmitter release in response to step depolarizations. Ribbon disruption has profound and specific effects on the kinetics of neurotransmitter release (Frank et al., 2010; Khimich et al., 2005; Snellman et al., 2011) and responses to sensory stimuli (Allwardt et al., 2001; Buran et al., 2010; Dick et al., 2003). Similarly, diurnal changes in ribbon number correlate with changes in the size of the readily releasable pool in goldfish bipolar cells (Hull et al., 2006). The effects on mIEPSCs have not previously been studied, however. Here, we examined the influence of the ribbon on mIEPSC amplitude and frequency using two approaches: (1) using fluorophore-assisted light inactivation (FALI) to selectively and acutely damage the synaptic ribbon in mouse bipolar cells while recording effects on synaptic transmission postsynaptically; and (2) examining the effects of hibernation on ground squirrel cones, which causes the removal of most ribbon material from the membrane, leaving a short ribbon intact opposing postsynaptic cells (Remé and Young, 1977). Our results here show that (1) unlike neurotransmitter release evoked by steps to 0 mV, mIEPSC frequency was dramatically reduced by FALI before a subsequent depolarization; (2) FALI reduced the amplitude of mIEPSCs; and (3) the shortened ribbons of hibernating animals exhibited a significant reduction in mIEPSC frequency, with little effect on mIEPSC amplitude after accounting for the change in frequency. These results reveal differences in the ribbon-associated vesicle pools contributing to mIEPSCs at resting potentials and in response to voltage steps, and support an important role for the ribbon in coordinating multivesicular release.

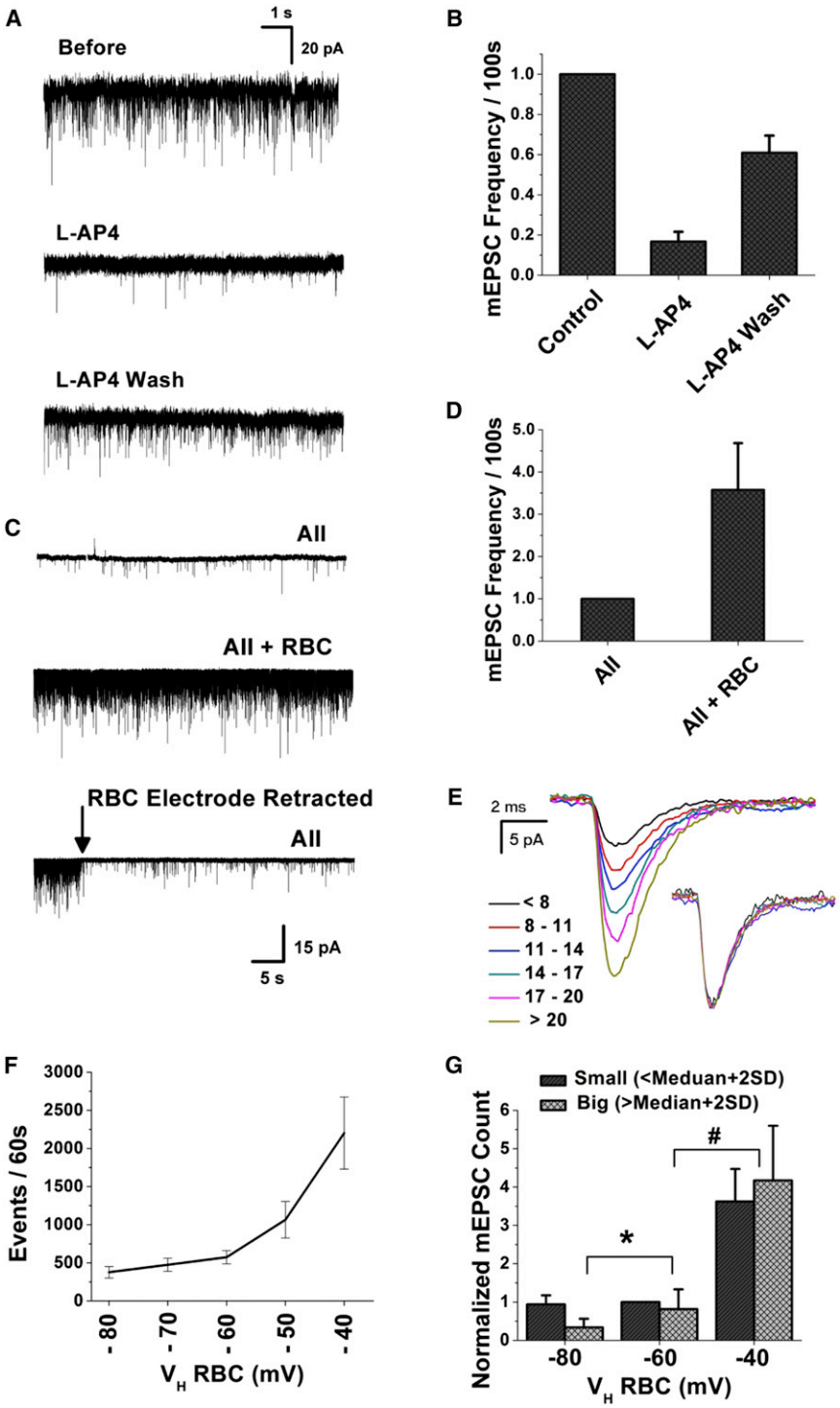

Figure 1. Nature of mIEPSCs in the RBC-AII Synapse

(A) mIEPSCs recorded from an AII before, in the presence of mGluR6 receptor agonist L-AP4 (4 μM), and upon washout of L-AP4.

(B) Bar graph showing effect of L-AP4 on mIEPSCs recorded from three AIIs normalized to the number of mIEPSCs recorded before L-AP4 addition. Before L-AP4 addition, we recorded an average of 1,219 mIEPSCs/min, which was reduced to 181 mIEPSCs/min upon L-AP4 addition.

(C) Voltage clamping a presynaptic RBC (VH −60mV) substantially increases the mIEPSCs recorded from the postsynaptic AII, and the effect is reversed upon killing the RBC.

(D) Bar graph showing normalized mIEPSC frequency from three experiments. Before voltage clamping the RBC, AIIs displayed, on average, 248 events/min in the presence of L-AP4.

(E) Average of over 30 mIEPSCs taken for different ranges of amplitude (indicated in legend) of mIEPSCs from a single paired recording. Inset shows the same traces normalized to their peak amplitudes. These average mIEPSCs show remarkable similarity in kinetics and waveform.

(F) Effect of bipolar cell holding potential on frequency of AII mIEPSCs (n = 7).

(G) Bar graph showing mIEPSC counts as small (mIEPSC amplitude < median + 2 SD) and big (mIEPSC amplitude > median + 2 SD) plotted for different holding potential of RBC (−80, −60, and −40 mV) from seven experiments. Each value is normalized to the number of small mIEPSCs at −60 mV for that particular recording. On average, we recorded 573 mIEPSCs/min with the bipolar cell held at −60 mV. There is a notable increase in the percentage of mIEPSCs with bigger amplitude at −40 mV of RBC's membrane potential (n = 7, $p < 0.001$; paired Student's t test). All VH = −60 mV and RBC VH = −60 mV, unless mentioned otherwise. The median and SD used to define large and small events were determined by the responses measured with the RBC held at −60 mV.

Error bars represent SEM.

RESULTS

Characterization of mIEPSCs at Rod Bipolar Cell to AII Amacrine Cell Synapse

To study the properties of mIEPSCs released from a ribbon-type synapse, we first performed whole-cell voltage clamp recordings of AII-Amacrine cells (AIIs) under conditions where GABAergic and glycinergic synaptic transmission had been blocked (see Experimental Procedures), without recording from a presynaptic RBC. Under these conditions, recordings (e.g., Figure 1A) from AIIs exhibit frequent AMPA receptor-mediated mIEPSCs (Mørkve et al., 2002; Veruki et al., 2003). Application of the mGluR6 agonist L-AP4, which hyperpolarizes ON-type bipolar cells (Slaughter and Miller, 1981), reduced the frequency of these events by >80% (Figures 1A and 1B), as previously reported (Singer et al., 2004). Upon voltage clamping a presynaptic RBC (V_H = −60mV) in the presence of 4 μM L-AP4, we observed a significant increase in the frequency of spontaneous mIEPSCs (Figures 1C and 1D), which was reversed upon killing the voltage-clamped RBC (Figure 1C). These results suggest that although each

rodent AII receives glutamatergic input from several RBCs (Kolb and Famiglietti, 1974; Sterling et al., 1988; Tsukamoto et al., 2001), under conditions of paired recordings in the presence of L-AP4, the spontaneous activity that is observed is dominated by input from the single voltage-clamped presynaptic RBC.

The mIEPSCs recorded in the AIIs exhibit considerable heterogeneity in amplitude, consistent with coordinated multivesicular release (Singer et al., 2004). Random superposition of mIEPSCs is unlikely to account for the heterogeneity in event sizes we observe. The highest frequency of mIEPSCs we observed when a presynaptic bipolar cell was held at a resting potential of −50 or −60 mV was 37 events/s. Assuming a stochastic process at this rate, we would expect only 3.7% of mIEPSCs to be followed within 1 ms by another event, which is well within our ability to detect events. At the average rate observed at −60 mV, the coincidence rate of events within 1 ms of another mIEPSC is less than 1% of all events. Similarly, if large mIEPSCs arise from stochastic coincidental release of multiple vesicles, then one might expect that large mIEPSCs might exhibit slower kinetics than smaller mIEPSCs. To test this idea, we grouped the mIEPSCs into six subgroups based on their amplitude and averaged a random selection of each subgroup. Figure 1E shows the average mIEPSC for each subgroup, and the inset shows the averages normalized to the peaks. The waveform and kinetics did not vary with amplitude (Figure 1E, inset), consistent with the idea that larger mIEPSCs are a result of multivesicular release from the presynaptic bipolar cell, supporting the findings of Singer et al. (2004).

We next looked at the effect of presynaptic holding potential on the amplitude and frequency of mIEPSCs. To do so, RBCs were held at membrane potentials between −80 and −40 mV for 100 s and mIEPSCs were analyzed. Since RBCs exhibit a phasic component of increased neurotransmitter release upon depolarization (Jarsky et al., 2011; Oesch and Diamond, 2011; Singer and Diamond, 2006; Snellman et al., 2009), we analyzed mIEPSC properties beyond 60 s after the initiation of a voltage step to assay the properties of steady-state release. As expected for the calcium dependence of neurotransmitter release, the steady-state mIEPSC frequency is dependent on the holding potential of the presynaptic RBC (Figure 1F), as previously described (Jarsky et al., 2011; Oesch and Diamond, 2011). In addition, we found that the amplitude of mIEPSCs also exhibited a strong voltage dependence. To simplify the analysis across cell pairs, which exhibit considerable variability in amplitude from pair to pair, we divided mIEPSCs into small and large events. Small mIEPSCs were defined as any event that was less than the median amplitude +2 SD at −80 mV for any particular cell pair. Large events were defined as events that were greater than the median +2 SD. Figure 1G plots the number of small and large events for bipolar cells held at −80, −60, and −40 mV normalized to the number of small events at −80 mV. As shown in Figure 1G, more positive membrane potentials favors bigger mIEPSCs.

Since mIEPSC frequency and amplitude both exhibited a strong voltage dependence, we next tested the extent to which calcium entry through calcium channels was required for mIEPSCs or for the triggering of large mIEPSC. To do so, we used the voltage-gated calcium channel blocker Co^{2+}. Figure 2A shows that 5 mM $CoCl_2$ was sufficient to block all evoked release in response to a voltage step to a presynaptic RBC, in our recordings, indicating effective block of voltage-gated calcium channels in the RBC. Of note, the opening of single calcium channels is sufficient to drive neurotransmitter release from RBCs (Jarsky et al., 2010), further supporting the idea that nearly all channels are blocked by $CoCl_2$ in these experiments. By contrast, mIEPSC frequency was only reduced ~60% by the addition of 5 mM $CoCl_2$ in pairs where the RBC was held at a membrane potential of −60 mV. Both the evoked release and mIEPSC frequency recovered following washout of $CoCl_2$ (Figures 2A–2C). We also performed experiments with the L-type calcium channel blocker nifedipine. With nifedipine (100–400 μM), we were only able to block evoked release by 58% ± 22% (n = 3 pairs), perhaps due to poor penetration of the compound into the slice. In qualitative agreement with the results with Co^{2+}, we found that the large reduction in evoked release was accompanied by a considerably small reduction in mIEPSC frequency (33% ± 5%; n = 5 cells). These results suggest that true calcium-channel independent "spontaneous" release represents a smaller fraction of the release that we observed when a presynaptic bipolar cell was held at −60 mV.

Also apparent in the results was that the addition of Co^{2+} reduced the amplitude of the mIEPSCs (e.g., Figure 2B), consistent with a role for calcium channels in coordinating multivesicular events (Graydon et al., 2011; Li et al., 2009). To analyze this effect, we measured the size of mIEPSCs in the presence and absence of $CoCl_2$ and found that blockade of calcium channels resulted in a dramatic reduction in the size of mIEPSCs (Figure 2D), with the mean amplitude reduced from 9.19 ± 0.07 pA to 6.69 ± 0.09 pA ($p < 0.001$). If one assumes that the mEPSCs observed in $CoCl_2$ represent the true spontaneous release from all presynaptic bipolar cells, then one can recover the component of release evoked from calcium entry through calcium channels by subtracting the $CoCl_2$ distribution from the distribution in the absence of channel blockers. Figure 2E shows those results from this analysis. From Figure 2E, one can see that calcium entry through calcium channels favors larger, presumptive multivesicular events. Similarly, partial blockade of calcium channels using nifedipine (100–400 μM) decreased the average mIEPSC size by 33.3% ± 7% (n = 4,502 events before nifedipine and 3,026 events after). Our results are consistent with a role for calcium channels in coordinating multivesicular release (Graydon et al., 2011), and are consistent with the idea that multivesicular release may provide a mechanism for distinguishing between true spontaneous mEPSCs and evoked mIEPSCs (Singer et al., 2004).

Effect of Synaptic Ribbon Damage on mIEPSCs

To test the role of the synaptic ribbon in mIEPSC release, we used fluorophore assisted light inactivation (FALI) (Hoffman-Kim et al., 2007) to selectively and acutely damage the ribbon (Snellman et al., 2011), while monitoring release postsynaptically in a postsynaptic AII. In brief, this method takes advantage of the generation of singlet oxygen molecules upon excitation of a fluorophore to generate local damage near the fluorophore. To selectively target the ribbon, we used the whole-cell patch electrode to load RBCs with fluorescein-conjugated short peptides

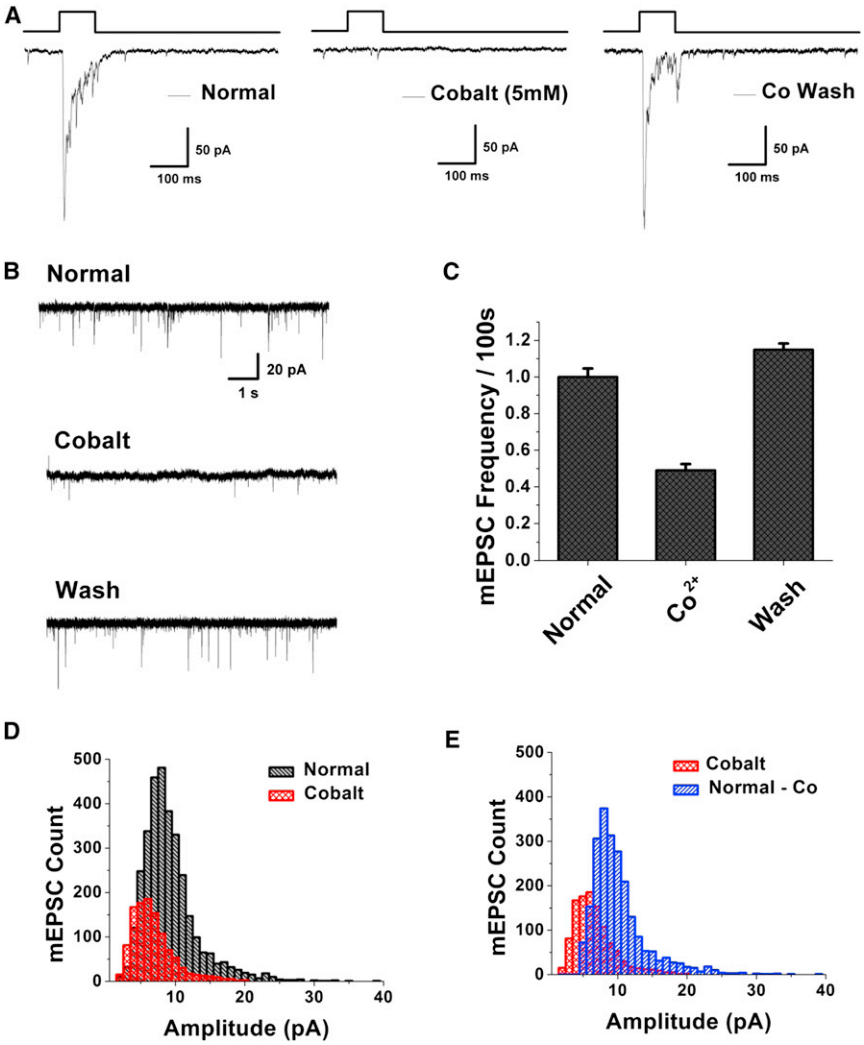

Figure 2. Opening of Voltage-Gated Calcium Channels Is Required for Multivesicular Release

In a double voltage-clamped RBC and AII pair, step depolarization of RBC from −60 to 0 mV triggers a postsynaptic EPSC recorded from the AII.

(A) Effect of 5 mM cobalt chloride ($CoCl_2$) on evoked release. Note that $CoCl_2$ reversibly blocks all evoked release from the RBC.

(B) Recording of mIEPSCs from an AII with RBC held at −60 mV, showing effect of $CoCl_2$ on amplitude of mIEPSCs.

(C) Bar graph showing the effect of $CoCl_2$ (5mM) on mIEPSC frequency from four experiments. In all four AII-RBC pairs, before $CoCl_2$ addition, the AII displayed 454 mIEPSCs/min, on average.

(D) Distribution of mIEPSC amplitudes before and after $CoCl_2$ addition. Note that results show significant reduction in the number of larger events upon $CoCl_2$ application (n = 4 pairs).

(E) Reduction in the distribution peak by two units on plotting subtracted mIEPSCs count before cobalt minus after $CoCl_2$, and mIEPSC counts with respect to their amplitude in presence of $CoCl_2$ (n = 4 pairs). AII VH = −60 mV, RBC VH = −60 mV. Error bars represent SEM.

that selectively bind to RIBEYE (Zenisek et al., 2004), the most abundant protein in synaptic ribbons (Schmitz et al., 2000). As reported earlier (Snellman et al., 2011), illumination of RBCs containing this peptide resulted in only a small reduction of the first evoked response following illumination, whereas the second response and consecutive responses were significantly reduced. By contrast, we observed a reduction in the frequency and amplitude of spontaneous mIEPSCs within seconds of the initiation of the FALI-inducing illumination (Figure 3B), when the RBC was held at a membrane potential of −60 mV. Unlike the evoked component (e.g., Figure 3C), the effect on mIEPSCs occurred prior to a depolarizing step (Figure 3B), suggesting that mIEPSCs arise from a separate ribbon-associated pool of vesicles than those involved in the transient response to depolarization. As a control, we performed similar experiments with cells loaded with a fluorescein-labeled scrambled peptide, and observed no change in the spontaneous or evoked release upon illumination (Figures 3F–3I). Figure 3E summarizes the effects of illumination on the frequency of mIEPSCs at −50 or −60 mV across 12 RBC:AII pairs with the ribbon binding peptide, and 2 RBC:AII pairs with the scrambled peptide (Figure 3J). For the 12 RBC:AII pairs (Figure 3E), the average absolute frequency observed per minute was 1087 ± 178 before FALI and 658 ± 101 after FALI.

Figure 4 investigates the effect of ribbon damage on the amplitude of mIEPSCs. Figure 4A shows the size of each mIEPSC before (black ●) and after (gray ◇) illumination of the ribbon-binding peptide for one experiment. As is apparent in Figure 4A, ribbon damage resulted in a dramatic reduction in the number of large mIEPSCs. Figure 4B shows a histogram of the mIEPSC sizes from the same experiment as in Figure 4A, whereas Figure 4C summarizes the results across 12 synaptic pairs. Figure 4C compares the effect of ribbon damage on small mIEPSCs (defined as less than median +2 SD before FALI) to the effect on large mIEPSCs. As shown in Figure 4C, illumination of the ribbon-bound peptide had a substantially greater effect on bigger mIEPSCs (reduced by 75%) than on small mIEPSCs (reduced by 20%). These results suggest that a functional ribbon is required for the coordination of multivesicular release.

If ribbon damage inflicts preferential loss of multivesicular release at resting potentials, then it may also hold true for depolarization-mediated multivesicular release, which has previously been described at the RBC:AII synapse (Singer et al., 2004). As described previously (Singer and Diamond, 2003; Singer et al., 2004; Snellman et al., 2011), a step depolarization to −10 mV to the presynaptic RBC evoked a characteristic postsynaptic response with a transient component followed by an asynchronous

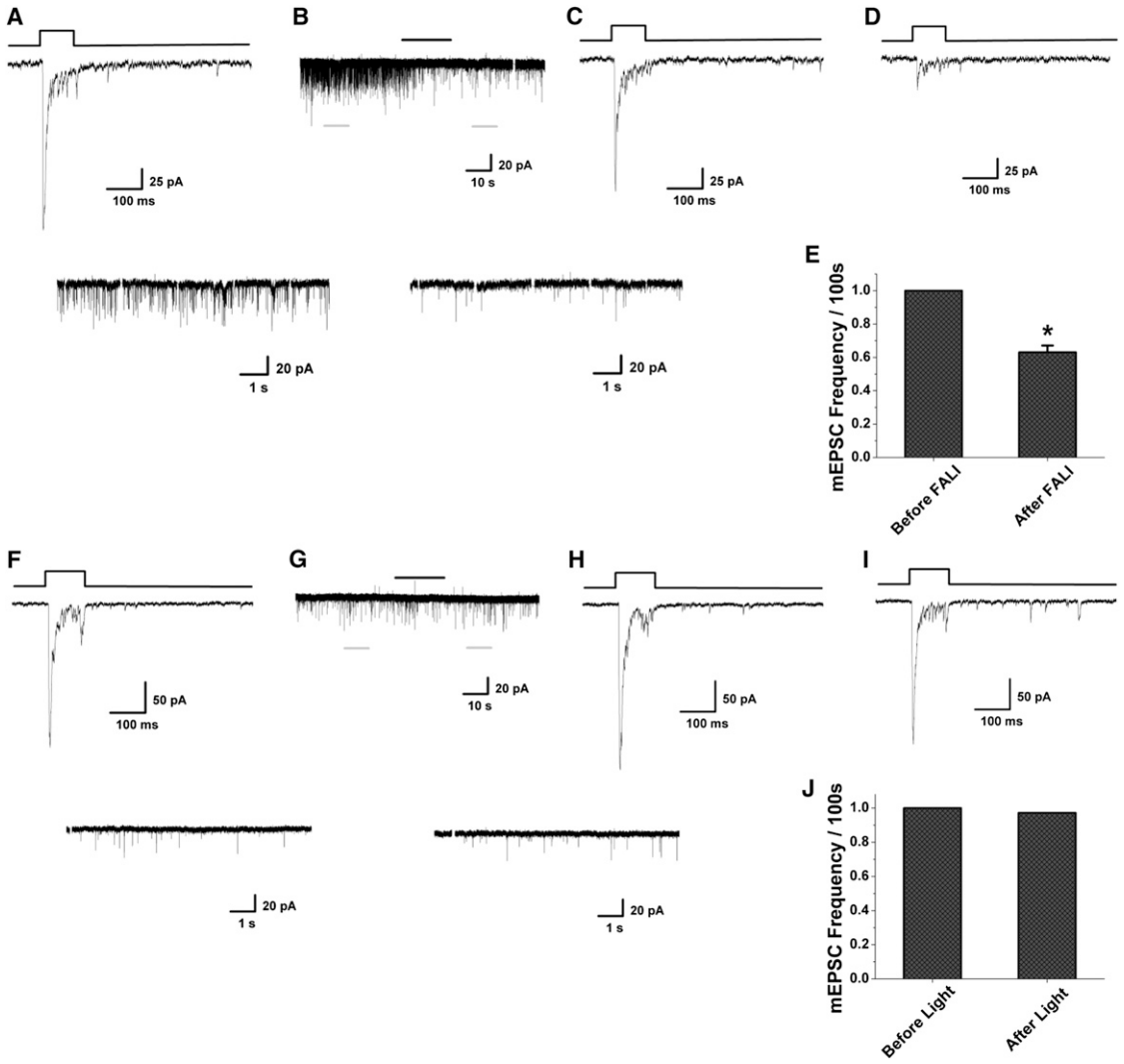

Figure 3. FALI of RIBEYE Affects Vesicle Release from Active Zone

(A) EPSCs observed in an AII upon depolarization of the synaptically connected RBC, filled with the ribbon-binding fluorescein-labeled peptide before FALI.

(B) Recording of mIEPSCs during period when FALI is induced by illumination with blue light (black bar), while bipolar cell is held at a membrane potential of −60 mV. Note that the mIEPSCs are rapidly affected during the 15 s illumination. Small gray bars indicate the inserts plotted from the 10 s recording, before and after FALI.

(C) The first evoked response after FALI from the same cell pair. Note that the response is similar to the evoked response before FALI (A), despite dramatic effect on mIEPSCs. On average, the EPSC in response to the first depolarization after FALI had a charge that was 81.1% ± 5.5% of the EPSC prior to illumination.

(D) The response to a second voltage step after FALI. Note that the amplitude is substantially reduced.

(E) Bar graph showing significant reduction in frequency of mIEPSCs after FALI from 12 RBC-AII pairs, normalized to the frequency of events before FALI (*$p < 0.001$; paired Student's t test).

(F–J) Same as (A)–(E), except with scrambled version of the peptide in the presynaptic pipette. No noticeable alteration in the frequency and amplitude of evoked EPSC or mIEPSCs was observed in the postsynaptic AII upon blue light stimulation (n = 2). VH RBC = −50 mV or −60mV; VH AII = −60 mV.

Error bars represent SEM.

or delayed component (Figure 4D). The asynchronous component shows distinct multiquantal events that have been described as a result of coordinated multivesicular release (Singer et al., 2004). The large events are particularly pronounced when the intracellular calcium buffer in the bipolar cell is reduced. Figure 4E compares the size of the mIEPSCs during the asynchronous phase of release measured before and after illumination of the ribbon-binding peptide, in pairs in which the RBC was filled with an internal solution with an EGTA concentration of 0.5 mM. In agreement with our earlier finding, ribbon damage resulted in preferential loss in the number of larger, presumably multivesicular, mIEPSCs ($p < 0.001$; paired Student's t test comparing fraction of large events). Figure 4F summarizes the results obtained from five experiments.

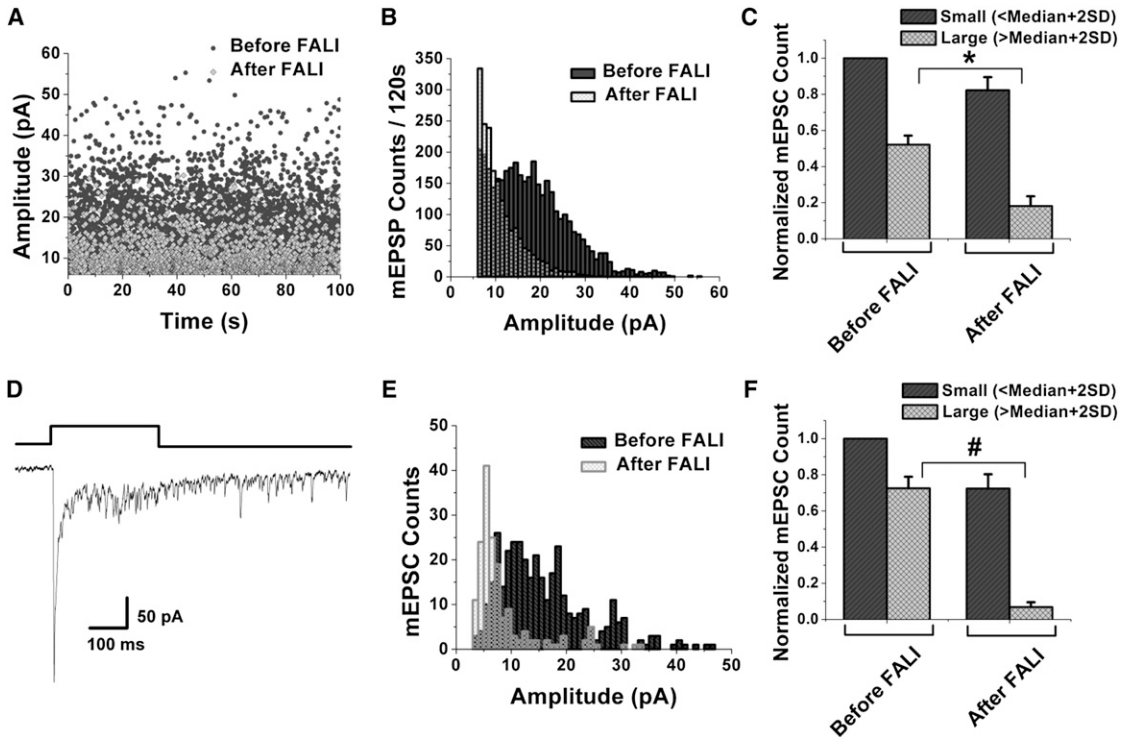

Figure 4. FALI Of Ribbons Affect Multivesicular Release

(A) Distribution of individual minis from a single experiment plotted over time, before (black ●) and after (gray ◇) FALI. Note that each dot represents the amplitude of a single mIEPSC.

(B) Overall mIEPSC histogram of event amplitude before (black) and after (gray) FALI for a single pair. Note the dramatic drop in the number of larger events observed.

(C) Normalized mIEPSC counts plotted as small (< median + 2 SD) and big (> median + 2 SD) before and after FALI from 11 RBC-AII pairs. A preferential loss of bigger amplitude mIEPSCs or multivesicular events is observed (C); n = 12 pairs, *p < 0.001; paired Student's t test). The median and SD were defined for each pair as response measured with the RBC held at −60 mV (n = 6) or −50 mV (n = 6) before FALI, and the overall data are normalized to the frequency of small mIEPSCs before FALI. Overall, the data presented in this panel come from six RBCs held at −50 mV, which contributed 7,663 mIEPSC before FALI and 4,487 mIEPSCs after FALI, and six RBCs held at −60 mV, which contributed 4,229 mIEPSCs before FALI and 2,801 after FALI.

(D) Postsynaptic response of an AII observed on stimulating the presynaptic RBC. The evoked EPSC display a fast transient component followed by an asynchronous component.

(E) Amplitude histogram of mIEPSC during asynchronous component of release from 5 AII-RBC pairs before and after FALI.

(F) Bar graph showing contribution of small (< median + 2 SD) and large (> Median + 2 SD) mIEPSCs, during asynchronous component of release (#p < 0.001; paired Student's t test). The median and SD were defined for each pair as asynchronous response measured upon depolarizing the RBC from a holding potential of −60 or −50 mV to 0 mV before FALI. The fast transient component and release observed during depolarization pulse to the RBC was not included for analysis. Error bars represent SEM.

Calcium-Channel Independent Release Is Insensitive to Ribbon Damage

In the presence of 5mM $CoCl_2$ (Figures 2B and 2C), a reduced number of small mIEPSCs remain, indicating that the majority of mIEPSCs observed in AIIs arise as a consequence of calcium influx through voltage-gated calcium channels. We tested whether the residual mIEPSC could be reduced by damage directed to the ribbon and whether the effect of FALI required calcium entry through calcium channels. We found that illuminating the ribbon-bound peptide had only modest effects on the frequency (Figure 5) and no effect on the amplitude ($p > 0.05$) of calcium-channel independent mIEPSCs in the presence of $CoCl_2$ (Figures 5A–5C). However, after a 5 min washout of $CoCl_2$, the mIEPSCs exhibited little recovery, indicating that illumination during the blockade of calcium channels was sufficient to affect mIEPSCs. These results suggest that a result of acute damage to the ribbon causes the specific loss of mIEPSCs that are dependant on calcium influx through voltage-gated channels.

Increasing mIEPSC Frequency after FALI Does Not Rescue Larger mIEPSCs

The preceding experiments described above indicate that acute damage to the synaptic ribbon reduces both the amplitude and frequency of mIEPSCs, but a key question is whether the change in amplitude is secondary to the effect on frequency. To dissociate the two effects, we took advantage of the relationship between membrane potential and mIEPSC frequency (Figure 1F) to match the frequencies before and after FALI. To do so, RBCs were held at membrane potentials varying between −70

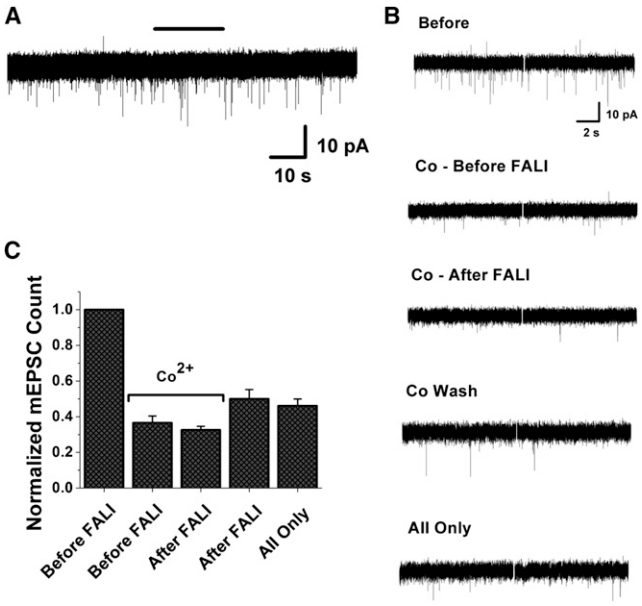

Figure 5. Calcium-Channel Independent Release Is Insensitive to FALI

(A) mIEPSCs recorded from the postsynaptic AII in presence of 5mM $CoCl_2$. The black bar indicates timing of 20 s blue light illumination to stimulate FALI.

(B) The 20 s records of mIEPSCs from the postsynaptic AII before $CoCl_2$ perfusion, in $CoCl_2$, after photodamge (PD) in $CoCl_2$, upon $CoCl_2$ washout, and after killing the presynaptic RBC.

(C) Bar graph showing the normalized mIEPSCs for three AII-RBC pairs displaying the effect of FALI in absence of calcium influx.

Error bars represent SEM.

and −45 mV before damage induction and between −50 and −40 mV after damage in 5 mV increments, while mIEPSCs were monitored in a synaptically connected AII. Figure 6A shows the normalized frequency of mIEPSCs recorded across six of eight RBC:AII pairs at a selection of potentials before and after the ribbon was damaged. From the normalized bar graph, the frequency of mIEPSCs at −55 mV before damage approximately matched that at −45 mV after damage for the same duration, and the amplitude of mIEPSCs were compared. In two of the eight RBC:AII pairs, depolarization of the RBC after FALI failed to increase the mIEPSC frequency to pre-FALI levels, and these pairs were not used for this analysis. Figure 6B shows the comparison of amplitude of events for a representative RBC:AII pair for RBC holding potential at −55 mV before FALI to −45 mV after FALI. As can be seen from Figure 6B, despite exhibiting similar mIEPSC frequencies, the amplitude of the events exhibited a dramatic shift toward smaller events. On plotting the normalized amplitude of events as small (< median + 2 SD) and big (> median + 2 SD) for six RBC:AII pairs, over 50% reduction in the number of big events was observed (Figure 6C). The mIEPSCs had an amplitude of 8.34 ± 0.11 pA before damage and 6.94 ± 0.09 pA after damage at a matching frequency. These results support the notion that ribbons are important regulators of multivesicular release, independent of its influence on mIEPSC frequency.

Recordings from Hibernating Ground Squirrel Indicate That Small Ribbons Exhibit Reduced mIEPSC Frequency, but Are Sufficient for Multivesicular Release

The results above support the idea that functional synaptic ribbons support multivesicular release in the RBC:AII synapse. To test whether ribbon size influences mIEPSC properties, we investigated mIEPSC amplitude and frequency in the control and hibernating ground squirrel cone synapses. Upon hibernation, much of the synaptic ribbon material in ground squirrel cones is sequestered away from the plasma-membrane in aggregates, leaving the synaptic release site with smaller synaptic ribbons that protrude a much shorter distance into the interior of the cone (Remé and Young, 1977). We hypothesized that the shrinking of ribbons in this preparation may also affect either the amplitude or frequency of mIEPSCs. To test this idea, we monitored mIEPSCs (mediated by AMPA receptors) in postsynaptic b2 Off cone bipolar cells in response to vesicle release from presynaptic cones in slices taken from hibernating and nonhibernating ground squirrel retinae. Figure 7 summarizes the results. The inset in Figure 7A confirms the previous results of Remé and Young (1977) and shows depletion of the major synaptic ribbon protein, RIBEYE, from the outer plexiform layer in hibernating animals. Recordings from retinas of hibernating animals exhibited a pronounced decrease in mIEPSC frequency (Figures 7A and 7D) and amplitude (Figures 7B and 7C), with no change in resting membrane potential (−44.5 ± 3.5 mV in control, n = 7; −43.0 ± 3.5 mV in hibernating animals, n = 7; carried out in current clamp), and no obvious change in the distribution of glutamate receptor localization (Figures 7E and 7F). The cone calcium currents were found to be slightly smaller in the hibernating tissues (peak amplitude when stepped from −70 mV to −20 mV: 97.5 ± 18.7 pA in control, n = 5; 81.2 ± 13.9 pA in hibernating animals, n = 5), but this difference was not statistically significant and there was no change in current-voltage relationship.

On average, the amplitude of the mIEPSCs was 60% smaller in hibernating squirrel retinas (Figures 7B and 7C), with no change in the kinetics of the individual events (Figure 7B, inset). An amplitude histogram revealed that the decrease in amplitude is the result of the specific loss of large-amplitude events (Figures 7D and 8B). To test whether the effect on mIEPSC size was secondary to the change in frequency, we next depolarized cones in paired cone-bipolar recordings to raise the frequency of mIEPSCs in bipolar cells in the hibernating squirrel retinas. After cone depolarization, both the frequency and amplitude of the bipolar mIEPSCs in the hibernating animals increased. However, even with continuous depolarization of cones, the bipolar mIEPSC frequency remained significantly lower than that in the awake tissues (Figure 8A, blue bar). Moreover, we were not able to further increase the frequency of mIEPSCs with presynaptic cone depolarization, higher extracellular Ca^{2+} concentration, or treatment of Bay K (10 μM), indicating that the large portion of the ribbon structure removed from the membrane during hibernation is critical for maintaining mIEPSC frequency. To match the frequencies of depolarized hibernating cones, we instead added 500 μM Co^{2+} to awake animals (Figure 8A, green bar). When compared with slices from awake animals that were treated with low concentration

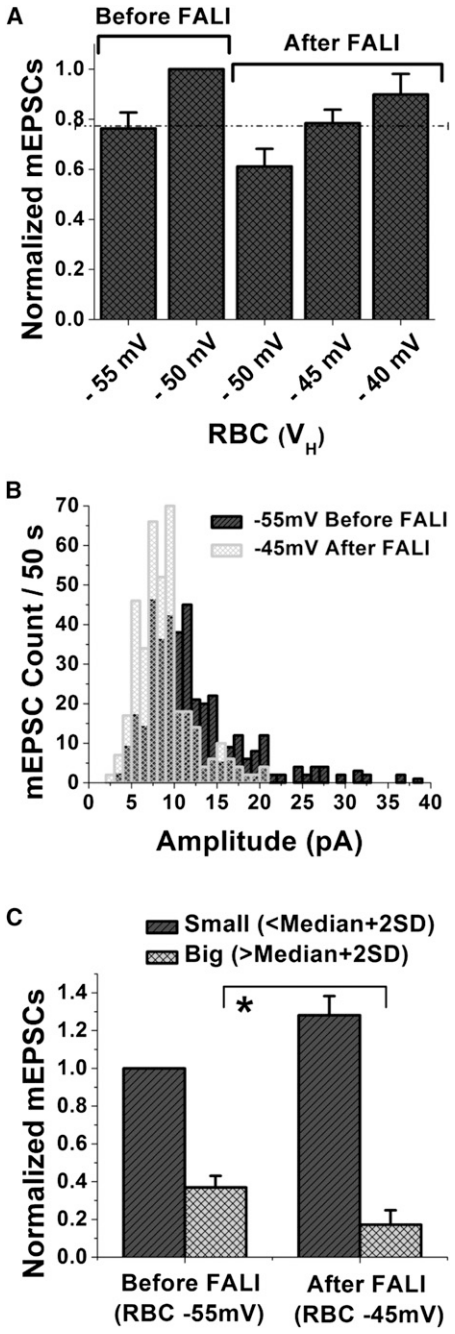

Figure 6. Increasing mIEPSC Frequency after FALI Does Not Rescue Larger mIEPSCs

(A) Bar graph of normalized mIEPSC frequencies recorded from AIIs plotted for different holding potentials of RBC, before and after FALI to ribbons (n = 6 RBC-AII pairs). FALI to ribbons was performed at while RBC was held at −70 mV. Dotted line indicates that mIEPSC frequency for −55 mV RBC holding potential before FALI is roughly equivalent to −45 mV RBC holding potential after FALI.

(B) Histogram of mIEPSC amplitude before FALI at the holding potential of RBC, −55 mV, and after FALI at a holding potential of −45 mV post-FALI for a representative experiment.

(C) Normalized mIEPSC counts plotted as small (< median + 2 SD) and large (> median + 2 SD) across six RBC-AII pairs at RBC holding potential of −55mV before FALI, and at −45 mV after FALI. For the purposes of this analysis, the median and SD was defined at a membrane potential of −55 mV before photobleach. Note that a significant drop in the number of multivesicular events was observed after FALI (*p < 0.01).

Error bars represent SEM.

of Co^{2+}, their amplitude distributions are essentially the same (Figure 8D). Evidently, the remaining small ribbons, which are limited to the very bottom compartment, are sufficient to support multivesicular release, but fail to support normal frequencies of mIEPSCs.

Although we did not measure a significant difference in calcium currents in awake and hibernating animals, even a small difference in calcium current, below our level of detection in these experiments, could have large effects on neurotransmitter release rates (Dodge and Rahamimoff, 1967). To test whether calcium current underlies the effects of hibernation on mIEPSC frequency, we used 100 μM Co^{2+} to modestly reduce calcium channel currents in awake animals. Reduction of the calcium current by approximately 20% (Figure 8E) resulted in a reduction of mIEPSC frequency by approximately 25% (Figure 8F) and a shift in the amplitude distribution of mIEPSC, as expected for the decrease in frequency (Figure 8G). By contrast, hibernating animals exhibited mIEPSC frequencies that were 90% less than awake animals (Figure 8A and dashed line in Figure 8F). Evidently, the reduction in calcium current cannot explain the reduction in mIEPSC frequency.

DISCUSSION

Functional Ribbons Play a Role in Setting Tonic mIEPSC Release Rates

Our results support the idea that the ribbon is important for setting rates of tonic release. The small ribbons of hibernating ground squirrels exhibit a dramatic decrease in mIEPSC frequency though calcium channels and resting potential remain largely unaffected, suggesting that tonic release is reduced with the loss of ribbon material from the synapse. Similarly, FALI-directed damage to the mouse bipolar cell ribbon causes an immediate drop in frequency of mIEPSCs, while having little effect on spontaneous calcium-channel independent rates of release. Together, these results indicate that synaptic ribbons, in some way, play a critical role in setting tonic release rates.

Evidence for Heterogeneity between Vesicle Pools on the Ribbon

In previous work, we showed that fluorophore-conjugated peptides containing a RIBEYE-binding motif can be used to selectively label synaptic ribbons (Zenisek et al., 2004). FALI using a fluorescein-conjugated RIBEYE-binding peptide has little effect on the release of a pool of vesicles that presumably populate the ribbon prior to illumination, though it prevents the release of vesicles that repopulate the ribbon following the stimulus (Snellman et al., 2011). Here, we show that FALI of bipolar cells loaded with the ribbon-binding peptide results in a rapid reduction of mIEPSC frequency at low membrane potentials (−60/−50 mV), prior to a subsequent stimulus (Figure 3B). These

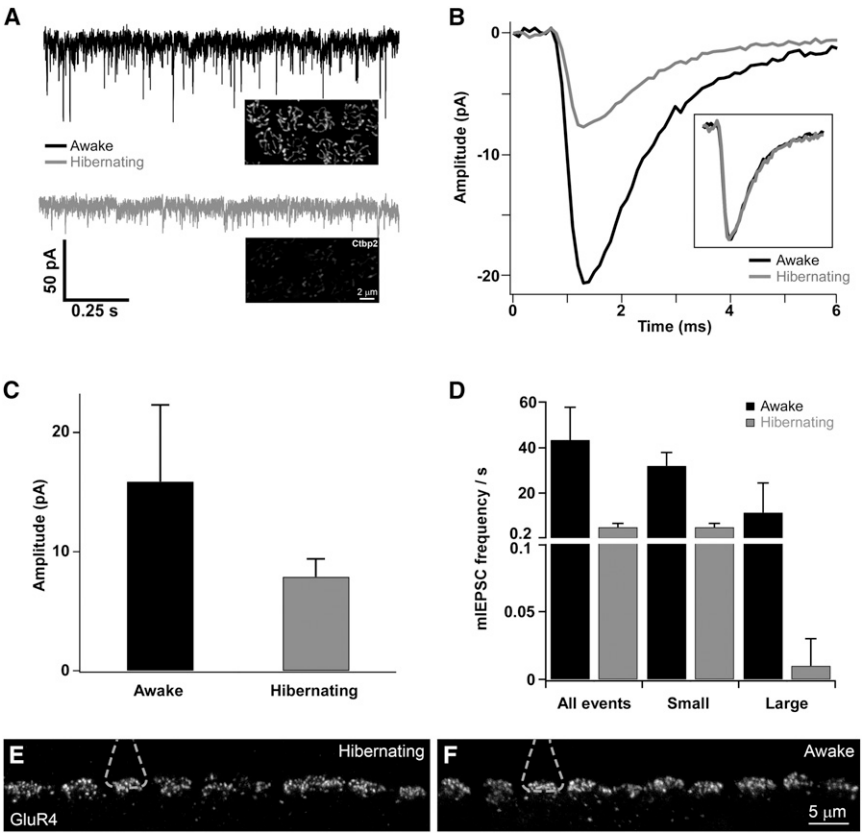

Figure 7. Hibernating Animals Show Decrease in the Size and Frequency of Spontaneous Release

(A) Sample traces of mIEPSCs recorded from b2 Off cone bipolar cells in retinal slices from awake and hibernating animals. Insets show immunolabeling of photoreceptor ribbons in whole mount of awake and hibernating tissues using Ctbp2 antibody.

(B) The amplitude of the average mIEPSC from hibernating animals is significantly smaller than that from awake ones, but with strikingly similar rise and decay kinetics (normalized waveforms shown in the inset).

(C) Bar graph showing the average mIEPSC amplitude recorded in awake (black; n = 1,982 events) and hibernating (gray; n = 595 events) animals. Error bars represent SD.

(D) There is a significant reduction in the frequency of mIEPSCs from hibernating animals (n = 4) compared to that from awake ones (n = 5), especially the large, putative multivesicular events. Note the change of y axis scale before and after the split. Error bars represent SEM.

(E and F) In retinal sections, immunolabeling of AMPA receptor subunit (GluR4) reveals no significant difference in expression level and distribution pattern between awake and hibernating tissues (n = 3 animals each). Dashed curves outline the location of exemplary cone terminals.

results suggest the existence of at least two ribbon-associated pools of vesicles: one pool that undergoes release at −50 to −60 mV, which is depleted within seconds of FALI, and one that is released by depolarizing steps to 0 mV. Since release at both low and high membrane potential is blocked by ribbon-directed FALI, we believe that both pools are ribbon associated, consistent with bassoon mutants, which exhibit fewer membrane-anchored ribbons and the parallel loss of spontaneous and evoked release from hair cells (Buran et al., 2010). Of note, recent studies in conventional synapses have demonstrated that spontaneous and evoked neurotransmission arises from largely independent pools of vesicles, which can be distinguished molecularly (Hua et al., 2011; Kavalali et al., 2011; Ramirez and Kavalali, 2011; Ramirez et al., 2012; Sara et al., 2011). A similar mechanism, with two parallel pools of vesicles for spontaneous and evoked release, both resident on the ribbon, could explain our results here. Alternatively, the different effects of FALI on mIEPSCs at −60 mV and evoked EPSCs could arise from heterogeneities in vesicle release probabilities, arising from either differences in proximity to calcium channels or differences in sensitivity to calcium (Burrone and Lagnado, 2000), such that a subset of vesicles are released at more negative potentials, whereas others can only be released in response to stronger stimuli. Such an explanation is plausible, because the FALI-driven loss of release appears to be use dependent (Snellman et al., 2011). A third model to explain our results is that the ribbon could act as a catalyst that facilitates vesicle exocytosis, by reducing the energy barrier in some way for neurotransmitter release. In this model, ribbon damage would increase the amount of calcium required to drive release and effectively prevent neurotransmitter release at low calcium concentrations, but have far less effect at more positive potentials, where calcium is sufficient to trigger the release process without aid of a functional ribbon. Further experiments will be necessary to distinguish between these mechanisms.

The Ribbon's Role in Multivesicular Release

Both AIIs in the mouse retina and Off cone bipolar cells in the ground squirrel retina show mIEPSCs with variable amplitude and strikingly similar waveforms and kinetics (e.g., Figures 1E and 7B; Singer et al., 2004; Veruki et al., 2003), similar to observations made postsynaptic to hair cell ribbon synapses (Glowatzki and Fuchs, 2002; Grant et al., 2010; Graydon et al., 2011; Li et al., 2009). Given the rapidity of the multivesicular events observed, these events are thought to represent the near-simultaneous release of the contents of multiple vesicles. We observed a substantial decrease in the amplitude of mIEPSCs in the presence of the calcium channel blocker, cobalt (Figure 2D), supporting the idea that opening of voltage-gated calcium channels near the ribbon is important for multivesicular release. Moreover, our results show that tonic depolarization causes a shift in the amplitude of mIEPSCs toward larger events, reminiscent of the voltage dependence observed postsynaptic to hair cells of the amphibian papilla (Li et al., 2009). These results are consistent with the idea that multivesicular release could be

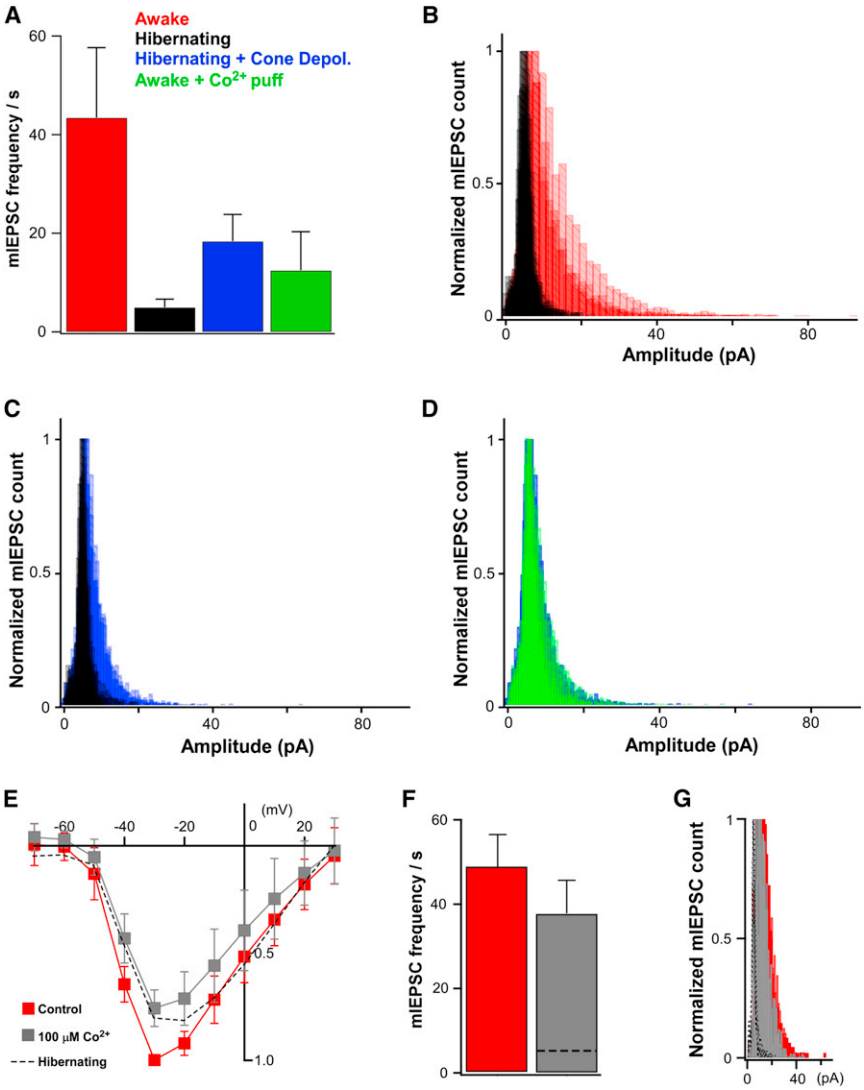

Figure 8. Increasing mIEPSC Frequency Does Elicit Larger mIEPSCs in Hibernating Animals

(A) mIEPSC frequency of bipolar cells under four different conditions: awake (n = 5; red), hibernating (n = 4; black), hibernating with presynaptic cone depolarization (n = 5; blue), and awake with low concentration (500 μM) of Co^{2+} (n = 5; green). Manipulations aimed to increase presynaptic release probability (such as depolarization of the presynaptic cone in paired recordings) did increase the frequency of mIEPSCs, but failed to reach the level of the awake condition. Thus, low concentration of Co^{2+} was applied to awake tissues to achieve a similar mIEPSC frequency as in hibernating tissues.

(B–D) Normalized histograms comparing mIEPSC amplitude distributions of different conditions. Larger events apparently can be elicited in hibernating tissues when the frequency of mIEPSCs is augmented.

(E) Current-voltage (I-V) curves show that 100 μM Co^{2+} reduced the peak amplitude of the cone Ca^{2+} currents by ~25% (24.1% ± 3.8%, n = 5) in retinal tissues from awake animals. The black dashed curve represents the I-V curve from hibernating tissues (normalized to the peak amplitude of the I-V curve from awake tissues).

(F) Under this condition, the frequency of mIEPSC dropped to a much lesser extent (21.5% ± 7.0%, n = 5) compared with hibernating tissues (dashed line).

(G) The distribution of the mIEPSC amplitude remained largely unchanged (dashed profiles depict mIEPSC distributions in hibernating tissues).

Error bars represent SEM.

a means of distinguishing synaptic noise generated by spontaneous release from tonic light-driven release (Singer et al., 2004), which may be important for signaling luminance levels by RBCs (Oesch and Diamond, 2011).

Evoked multivesicular release has been described in several conventional synapses, arising likely as a result of high release probability at some synapses in response to single action potentials (Auger et al., 1998; Biro et al., 2006; Christie and Jahr, 2006; Kirischuk et al., 1999; Tong and Jahr, 1994; Wadiche and Jahr, 2001). The multiquantal events described at ribbon-type synapses differ in that event synchrony persists in the absence of an action potential (Glowatzki and Fuchs, 2002; Li et al., 2009; Singer et al., 2004). Two theories have been proposed to explain multivesicular release at ribbon synapses: compound fusion of synaptic vesicles prior to exocytosis with the plasma-membrane (Matthews and Sterling, 2008), and coordinated fusion of several docked vesicles at the plasma membrane (Singer et al., 2004). In some hair cells, multivesicular events have been suggested to arise from calcium nanodomains near open calcium channels (Graydon et al., 2011). In rodent RBCs, however, multiquantal events can persist for hundreds of milliseconds after calcium channels are closed (Singer et al., 2004), suggesting some other mechanism for synchronizing events. We show here that damage directed to the entire ribbon by FALI reduces the amplitude of mIEPSCs, and that this reduction in mIEPSC amplitude persists even after accounting for changes in mIEPSC frequency. In contrast, the residual ribbons in hibernating ground squirrel cones remain capable of generating multivesicular events (Figure 8), while exhibiting a dramatic decrease in mIEPSC frequency. Hibernating animals retain a small ribbon that is dramatically reduced in height, but continues to be attached to the plasma membrane (Remé and Young, 1977). We suggest that longer ribbons that penetrate deeper into the cell are important for supporting mIEPSC rates, perhaps by ensuring that a large number of preprimed vesicles are available for release, but that multivesicular release requires only the base of the ribbon that associates with the plasma membrane.

It should be noted that some large events were still observed after FALI, albeit infrequently, which could reflect incomplete damage to the ribbon (Snellman et al., 2011), or could suggest that the ribbon supports multivesicular release but is not required

for it. The effects of FALI on mIEPSC size could alternatively be explained by a role for the ribbon in packing synaptic vesicles with neurotransmitter or with the coordination of multivesicular release. Although our results cannot distinguish between these two mechanisms, we favor the idea that the ribbon coordinates multivesicular release, based on the abundance of literature supporting multivesicular release from ribbon-type cells and the lack of evidence suggesting a role for the ribbon in vesicle packing.

EXPERIMENTAL PROCEDURES

Mouse Retinal Slice Preparation and Solutions

Retinal slices were prepared from 4- to 6-week-old C57/BL6 mice (Harlan). All procedures were approved by the Yale University Animal Care and Use Committee. Mice were anaesthetized with halothane (Sigma), sacrificed by cervical dislocation, and their eyes removed and enucleated. Whole retinas were isolated and placed on a 0.45 micron cellulose acetate/nitrate membrane filter (Millipore), which was secured with vacuum grease to a glass slide adjacent to the recording chamber. Slices were cut to a thickness of 150 μm using a tissue slicer, and transferred to the recording chamber while remaining submerged. The recording chamber was immediately attached to a perfusion system, and the slices were perfused at a rate of 5 ml/min with Ames media bubbled with 95% O_2 and 5% CO_2. The Ames media was supplemented with 100 μM picrotoxin and 50 μM 1, 2, 5, 6-Tetrahydropyridin-4yl methylphosphinic acid (TPMPA) to block GABAA and GABAC receptors, 10 μM strychnine to block glycine receptors, and 4 μM L-AP4 to hyperpolarize On bipolar cells. The standard recording solution for RBCs was composed of (in mM): 108 gluconic acid, 2 EGTA, 10 CsCl, 10 TEA, 4 MgATP, 1LiGTP. For FALI experiments, 1 mM of the free radical scavenger glutathione was included in the recording solution. For experiments looking at asynchronous release following step depolarizations to −10 mV, the EGTA concentration was reduced to 0.5 mM. The Amacrine cell internal solution was composed of (in mM): 100 CsCH3SO3, 10 EGTA, 20 TEA, 10 HEPES, 4 MgATP. 2 mM QX314 was added to block action potentials. The pH was adjusted to 7.4 with CsOH. The osmolarity of both extracellular and intracellular solutions was 289-297, with a pH of 7.35–7.40. All chemicals were obtained from Sigma, except for L-AP4, TPMPA (Tocris) and ribbon-binding peptides (Genscript). Glutathione was stored as a powder at 4°C, and was added to the pipette solution immediately before use. L-AP4 was stored as a stock solution at 4°C and was added to the bath solution at the day of experimentation. All other drugs were aliquoted, stored at −20°C, and dissolved in the pipette solution on the day of use.

Ground Squirrel Retinal Slice Preparation

All animal procedures were approved by the Animal Care and Use Committee of the National Eye Institute. The procedures for making ground squirrel retinal slices have been described previously (Li and DeVries, 2006). During recording, the tissue was superfused with bicarbonate buffered Ames media (Sigma-Aldrich) containing picrotoxin (50 μM) and Strychnine (10 μM). The pipette solution contained (in mM): CsCH3SO, 120; $MgSO_4$, 2; HEPES 10; TEA 20; EGTA 5; ATP 3; GTP 1; and Neurobiotin (Vector Laboratories), 0.1. pH was adjusted to 7.4 with CsOH. Slices were mounted on a Zeiss Examiner 1D microscope and superfused continuously at room temperature. Recordings were obtained with Axopatch 200B amplifiers (Molecular Devices), and currents low-pass filtered at 1 or 5 kHz using the 4 pole Bessel filter on the amplifier. The input/series resistances of the cone and bipolar cell recordings were approximately 1 GΩ/ < 20 MΩ and 0.8 GΩ/ < 20 MΩ, respectively. Data were digitized at 10 kHz using an ITC-18 interface (HEKA) controlled by a Dell computer running IgorPro 6.0 (WaveMetrics). Data were analyzed with custom-made software (IgorPro 6.0) and MiniAnalysis (Synaptosoft). In voltage clamp experiments, cone, bipolar, and Amacrine cell membrane voltages were maintained at −70 mV unless otherwise indicated.

Immunocytochemistry

Retinal tissues were fixed and processed for immunocytochemistry as previously described (Li and DeVries, 2006). Antibodies to the following were used: GluR4 (1:100; Millipore) and Ctbp2 (1:500; BD Biosciences). Tissues were mounted and imaged in the vertical or flat-mount orientation. Images were acquired with a LSM-510 confocal microscope (Zeiss) and edited with Zeiss Zen software and Photoshop CS4 (Adobe Systems). An α-Plan-Apochromat 63×/1.40 oil immersion lens was used.

Data Acquisition

Patch pipettes of resistance 8–11 MΩ were fabricated from borosilicate glass (TWF150-4, WPI) using a two-stage vertical puller (Narishige). Pipettes were coated with Sticky Wax to reduce noise (Kerr Corp). Whole-cell recordings were obtained using a dual EPC10 amplifier (HEKA Instruments). The input/series resistances of the RBC and AII recordings were approximately 3 GΩ/ 15-20 MΩ, and 1 GΩ/ < 40 MΩ, respectively. Cells were discarded if the holding current changed suddenly. Holding potentials were corrected for the liquid junction potential, which was measured to be approximately −12 mV depending on solutions. Slices were viewed with a Zeiss Axioskop 2FS plus equipped with a water-immersion 40× DIC objective. RBCs and AIIs were confirmed by their shape and position in the slice, as determined by fluorescent imaging of dye filled cells. FALI was performed using X-Cite 120Q (EXFO, Ontario, Canada) with a 488 nm band-pass excitation filter (Chroma). Data were acquired using PatchMaster software (HEKA Instruments). mIEPSCs were recorded for 60–120 s for each presynaptic holding potential. Currents were elicited at 60 s intervals, collected at 20 kHz, and low-pass filtered at 1 kHz. RBC calcium currents were leak subtracted using a p/4 protocol.

Analysis

Analysis was performed using IgorPro (WaveMetrics), MiniAnalysis (Synaptosoft), and Origin 7.5 (Microcal). Candidate mIEPSCs and evoked asynchronous mIEPSCs were detected automatically with MiniAnalysis using a threshold of 3–8 pA, depending on the noise level, and then subsequently confirmed by eye. Data are presented as means ± SEM (n = number of cells or events). mIEPSCs and asynchronous EPSCs are categorized as small or big based on the number of events less than or greater than the median of events plus 2 SD. Statistical significance was determined using a Student's t test, and differences were considered significant at the $p < 0.05$ level. The current traces shown in the figures represent individual traces.

ACKNOWLEDGMENTS

This work was funded by the National Institutes of Health (grant no. EY014990, to D.Z.) and the National Eye Institute Intramural Research Program (W.L.).

Accepted: November 12, 2012
Published: February 6, 2013

REFERENCES

Allwardt, B.A., Lall, A.B., Brockerhoff, S.E., and Dowling, J.E. (2001). Synapse formation is arrested in retinal photoreceptors of the zebrafish nrc mutant. J. Neurosci. *21*, 2330–2342.

Auger, C., Kondo, S., and Marty, A. (1998). Multivesicular release at single functional synaptic sites in cerebellar stellate and basket cells. J. Neurosci. *18*, 4532–4547.

Biro, A.A., Holderith, N.B., and Nusser, Z. (2006). Release probability-dependent scaling of the postsynaptic responses at single hippocampal GABAergic synapses. J. Neurosci. *26*, 12487–12496.

Buran, B.N., Strenzke, N., Neef, A., Gundelfinger, E.D., Moser, T., and Liberman, M.C. (2010). Onset coding is degraded in auditory nerve fibers from mutant mice lacking synaptic ribbons. J. Neurosci. *30*, 7587–7597.

Burrone, J., and Lagnado, L. (2000). Synaptic depression and the kinetics of exocytosis in retinal bipolar cells. J. Neurosci. *20*, 568–578.

Christie, J.M., and Jahr, C.E. (2006). Multivesicular release at Schaffer collateral-CA1 hippocampal synapses. J. Neurosci. *26*, 210–216.

Dick, O., tom Dieck, S., Altrock, W.D., Ammermüller, J., Weiler, R., Garner, C.C., Gundelfinger, E.D., and Brandstätter, J.H. (2003). The presynaptic active

zone protein bassoon is essential for photoreceptor ribbon synapse formation in the retina. Neuron *37*, 775–786.

Dodge, F.A., Jr., and Rahamimoff, R. (1967). Co-operative action a calcium ions in transmitter release at the neuromuscular junction. J. Physiol. *193*, 419–432.

Fatt, P., and Katz, B. (1952). Spontaneous subthreshold activity at motor nerve endings. J. Physiol. *117*, 109–128.

Frank, T., Rutherford, M.A., Strenzke, N., Neef, A., Pangršič, T., Khimich, D., Fejtova, A., Gundelfinger, E.D., Liberman, M.C., Harke, B., et al. (2010). Bassoon and the synaptic ribbon organize Ca^{2}+ channels and vesicles to add release sites and promote refilling. Neuron *68*, 724–738.

Glowatzki, E., and Fuchs, P.A. (2002). Transmitter release at the hair cell ribbon synapse. Nat. Neurosci. *5*, 147–154.

Grant, L., Yi, E., and Glowatzki, E. (2010). Two modes of release shape the postsynaptic response at the inner hair cell ribbon synapse. J. Neurosci. *30*, 4210–4220.

Graydon, C.W., Cho, S., Li, G.L., Kachar, B., and von Gersdorff, H. (2011). Sharp Ca(2) nanodomains beneath the ribbon promote highly synchronous multivesicular release at hair cell synapses. J. Neurosci. *31*, 16637–16650.

Hoffman-Kim, D., Diefenbach, T.J., Eustace, B.K., and Jay, D.G. (2007). Chromophore-assisted laser inactivation. Methods Cell Biol. *82*, 335–354.

Hua, Z., Leal-Ortiz, S., Foss, S.M., Waites, C.L., Garner, C.C., Voglmaier, S.M., and Edwards, R.H. (2011). v-SNARE composition distinguishes synaptic vesicle pools. Neuron *71*, 474–487.

Hull, C., Studholme, K., Yazulla, S., and von Gersdorff, H. (2006). Diurnal changes in exocytosis and the number of synaptic ribbons at active zones of an ON-type bipolar cell terminal. J. Neurophysiol. *96*, 2025–2033.

Jackman, S.L., Choi, S.Y., Thoreson, W.B., Rabl, K., Bartoletti, T.M., and Kramer, R.H. (2009). Role of the synaptic ribbon in transmitting the cone light response. Nat. Neurosci. *12*, 303–310.

Jarsky, T., Tian, M., and Singer, J.H. (2010). Nanodomain control of exocytosis is responsible for the signaling capability of a retinal ribbon synapse. J. Neurosci. *30*, 11885–11895.

Jarsky, T., Cembrowski, M., Logan, S.M., Kath, W.L., Riecke, H., Demb, J.B., and Singer, J.H. (2011). A synaptic mechanism for retinal adaptation to luminance and contrast. J. Neurosci. *31*, 11003–11015.

Kavalali, E.T., Chung, C., Khvotchev, M., Leitz, J., Nosyreva, E., Raingo, J., and Ramirez, D.M. (2011). Spontaneous neurotransmission: an independent pathway for neuronal signaling? Physiology (Bethesda) *26*, 45–53.

Khimich, D., Nouvian, R., Pujol, R., Tom Dieck, S., Egner, A., Gundelfinger, E.D., and Moser, T. (2005). Hair cell synaptic ribbons are essential for synchronous auditory signalling. Nature *434*, 889–894.

Kirischuk, S., Veselovsky, N., and Grantyn, R. (1999). Relationship between presynaptic calcium transients and postsynaptic currents at single gamma-aminobutyric acid (GABA)ergic boutons. Proc. Natl. Acad. Sci. USA *96*, 7520–7525.

Kolb, H., and Famiglietti, E.V. (1974). Rod and cone pathways in the inner plexiform layer of cat retina. Science *186*, 47–49.

Li, G.L., Keen, E., Andor-Ardo, D., Hudspeth, A.J., and von Gersdorff, H. (2009). The unitary event underlying multiquantal EPSCs at a hair cell's ribbon synapse. J. Neurosci. *29*, 7558–7568.

Li, W., and DeVries, S.H. (2006). Bipolar cell pathways for color and luminance vision in a dichromatic mammalian retina. Nat. Neurosci. *9*, 669–675.

Matthews, G., and Sterling, P. (2008). Evidence that vesicles undergo compound fusion on the synaptic ribbon. J. Neurosci. *28*, 5403–5411.

Matthews, G., and Fuchs, P. (2010). The diverse roles of ribbon synapses in sensory neurotransmission. Nat. Rev. Neurosci. *11*, 812–822.

Mørkve, S.H., Veruki, M.L., and Hartveit, E. (2002). Functional characteristics of non-NMDA-type ionotropic glutamate receptor channels in AII amacrine cells in rat retina. J. Physiol. *542*, 147–165.

Oesch, N.W., and Diamond, J.S. (2011). Ribbon synapses compute temporal contrast and encode luminance in retinal rod bipolar cells. Nat. Neurosci. *14*, 1555–1561.

Ramirez, D.M., and Kavalali, E.T. (2011). Differential regulation of spontaneous and evoked neurotransmitter release at central synapses. Curr. Opin. Neurobiol. *21*, 275–282.

Ramirez, D.M., Khvotchev, M., Trauterman, B., and Kavalali, E.T. (2012). Vti1a identifies a vesicle pool that preferentially recycles at rest and maintains spontaneous neurotransmission. Neuron *73*, 121–134.

Remé, C.E., and Young, R.W. (1977). The effects of hibernation on cone visual cells in the ground squirrel. Invest. Ophthalmol. Vis. Sci. *16*, 815–840.

Sara, Y., Bal, M., Adachi, M., Monteggia, L.M., and Kavalali, E.T. (2011). Use-dependent AMPA receptor block reveals segregation of spontaneous and evoked glutamatergic neurotransmission. J. Neurosci. *31*, 5378–5382.

Schmitz, F. (2009). The making of synaptic ribbons: how they are built and what they do. Neuroscientist *15*, 611–624.

Schmitz, F., Königstorfer, A., and Südhof, T.C. (2000). RIBEYE, a component of synaptic ribbons: a protein's journey through evolution provides insight into synaptic ribbon function. Neuron *28*, 857–872.

Singer, J.H., and Diamond, J.S. (2003). Sustained Ca2+ entry elicits transient postsynaptic currents at a retinal ribbon synapse. J. Neurosci. *23*, 10923–10933.

Singer, J.H., and Diamond, J.S. (2006). Vesicle depletion and synaptic depression at a mammalian ribbon synapse. J. Neurophysiol. *95*, 3191–3198.

Singer, J.H., Lassová, L., Vardi, N., and Diamond, J.S. (2004). Coordinated multivesicular release at a mammalian ribbon synapse. Nat. Neurosci. *7*, 826–833.

Slaughter, M.M., and Miller, R.F. (1981). 2-amino-4-phosphonobutyric acid: a new pharmacological tool for retina research. Science *211*, 182–185.

Snellman, J., Zenisek, D., and Nawy, S. (2009). Switching between transient and sustained signalling at the rod bipolar-AII amacrine cell synapse of the mouse retina. J. Physiol. *587*, 2443–2455.

Snellman, J., Mehta, B., Babai, N., Bartoletti, T.M., Akmentin, W., Francis, A., Matthews, G., Thoreson, W., and Zenisek, D. (2011). Acute destruction of the synaptic ribbon reveals a role for the ribbon in vesicle priming. Nat. Neurosci. *14*, 1135–1141.

Sterling, P., Freed, M.A., and Smith, R.G. (1988). Architecture of rod and cone circuits to the on-beta ganglion cell. J. Neurosci. *8*, 623–642.

Tong, G., and Jahr, C.E. (1994). Multivesicular release from excitatory synapses of cultured hippocampal neurons. Neuron *12*, 51–59.

Tsukamoto, Y., Morigiwa, K., Ueda, M., and Sterling, P. (2001). Microcircuits for night vision in mouse retina. J. Neurosci. *21*, 8616–8623.

Veruki, M.L., Mørkve, S.H., and Hartveit, E. (2003). Functional properties of spontaneous EPSCs and non-NMDA receptors in rod amacrine (AII) cells in the rat retina. J. Physiol. *549*, 759–774.

Wadiche, J.I., and Jahr, C.E. (2001). Multivesicular release at climbing fiber-Purkinje cell synapses. Neuron *32*, 301–313.

Zenisek, D., Horst, N.K., Merrifield, C., Sterling, P., and Matthews, G. (2004). Visualizing synaptic ribbons in the living cell. J. Neurosci. *24*, 9752–9759.